doi:10.1038/nature10870

Supplementary Notes

The overall expression level of all mutants was assessed by GFP-fluorescence and confocal microscopy (Supplementary Fig. S7); we further quantified membrane expression, permeation properties, and gating properties for the mutants.

Extensive analysis of the ion-conducting pathway could involve mutational alteration of ion selectivity, identification of sites required for pore-blocking ligands, and crystallographic detection of ions in the pore. Except for ion selectivity, the other experiments are (for ChRs) either not possible to obtain or beyond present ready capability for the following reasons. 1) there are no known and well-characterized pore blockers; 2) despite considerable effort, we have thus far not succeeded in obtaining reliable detection of ions at any site (ChR allows both monovalent and divalent cations to pass with little selectivity, likely contributing to difficulty in trapping a snapshot in which the translocating ion is tightly coordinated by charged residues along the pore); and 3) due to extremely small currents in ChRs there has not yet been direct assessment of ChR single channel activity. Therefore we analyzed ion selectivity from mutants of polar residues along the putative pathway that express well (Supplementary Fig. 12), and found as predicted that all mutants but E140A altered ion selectivity, supporting the crystallographic localization of the cation-conducting pathway.

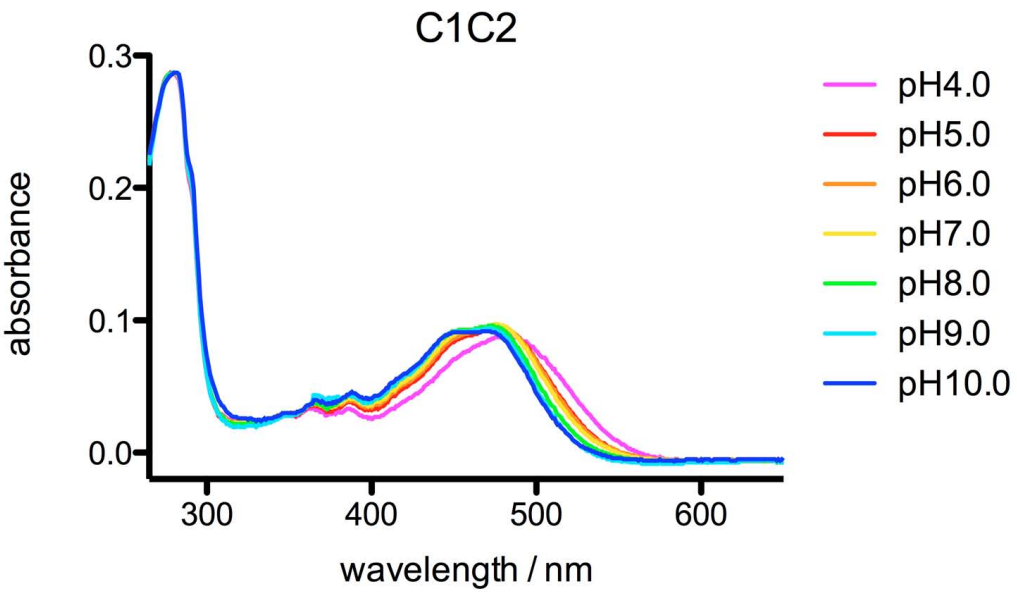

Supplementary Figure 1 | Absorption spectrum of purified C1C2 at different pH values. Absorption spectrum of recombinant C1C2 (in dodecyl maltoside solution) in the dark-adapted state at pH 4.0 (pink line), pH 5.0 (red line), pH 6.0 (orange line), pH 7.0 (yellow line), pH 8.0 (green line), pH 9.0 (cyan line), pH 10.0 (blue line), normalized to the absorption at 280 nm.

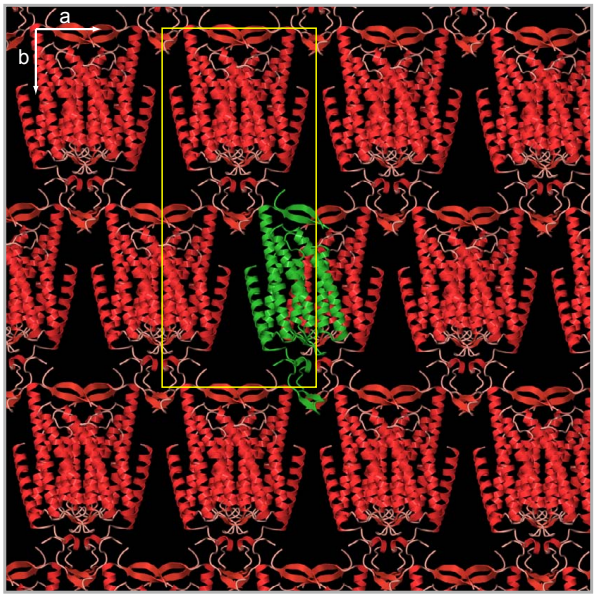

Supplementary Figure 2 | C1C2 crystal packing in the unit cell. Molecules in the C1C2 crystal lattice viewed perpendicular to the *a* – *b* plane. A C1C2 monomer is shown in green and other C1C2 molecules are shown in red.

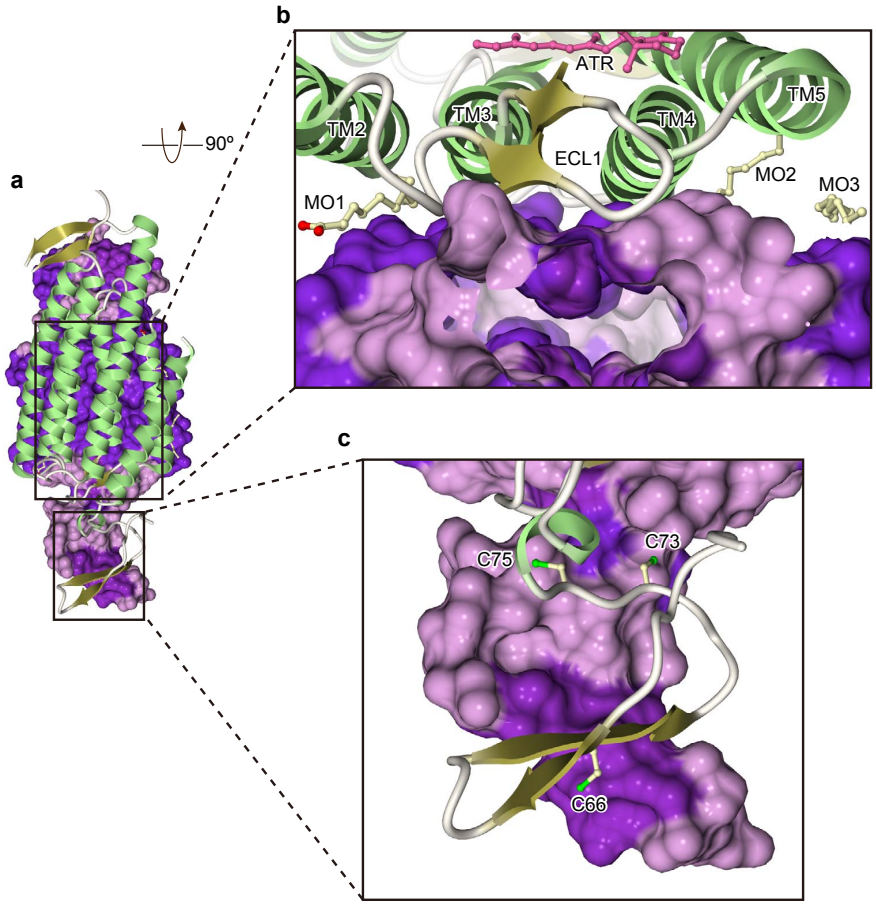

Supplementary Figure 3 | Dimer interface. a, Dimer interface between two monomers, with one monomer shown in a surface representation (magenta) and the other in a ribbon representation (green and yellow). **b,** Expanded view from (**a**), highlighting the interactions between TM3 and 4, and ECL1s. Monooleins are depicted by stick models. **c,** Expanded view from (**a**), highlighting the interactions between the N-domains, including Cys66 (27), Cys73 (34), and Cys75 (36).

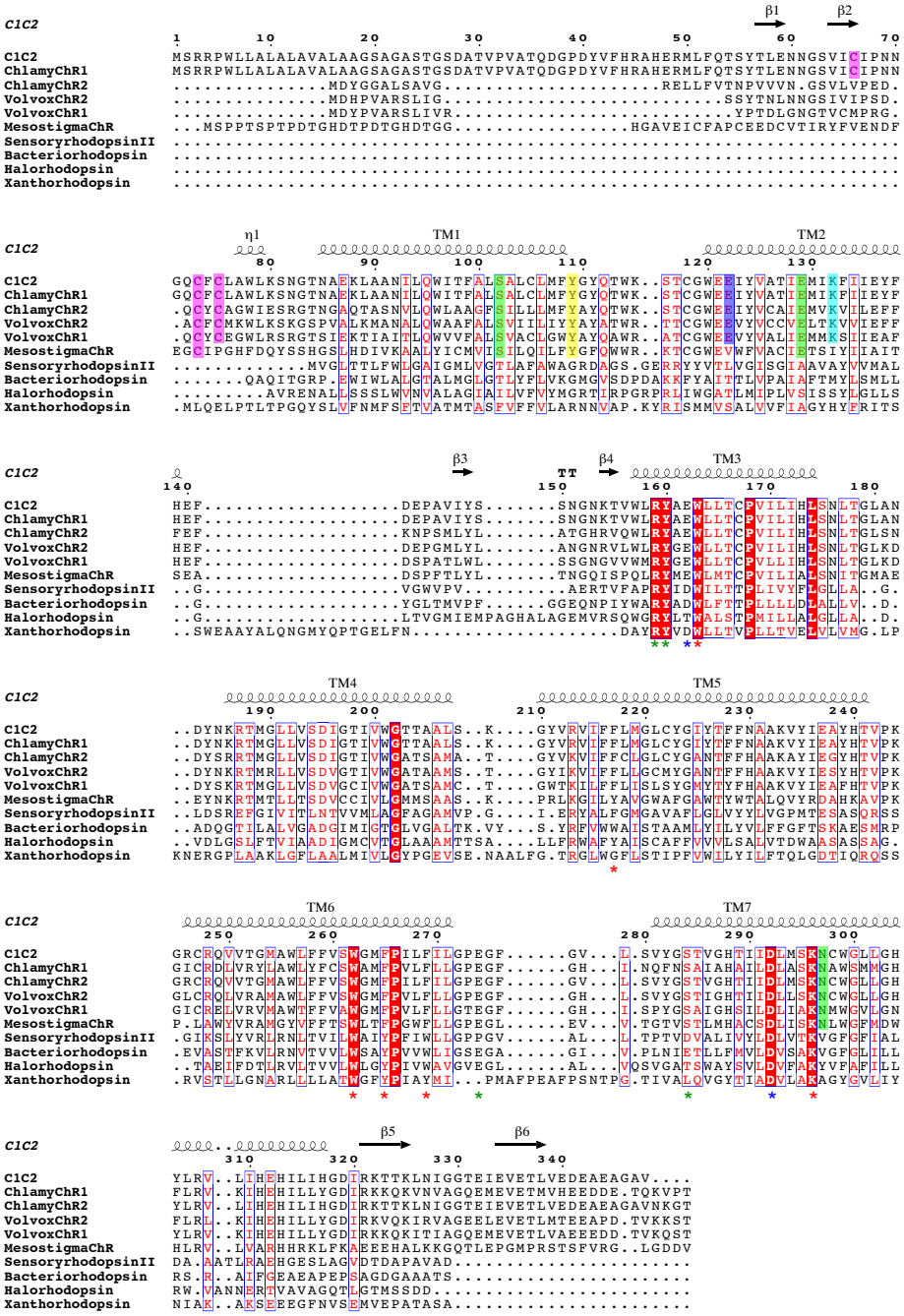

Supplementary Figure 4 | Structure-based sequence alignment. Shown are the C1C2 construct, ChR1 from *Chlamydomonas reinhardtii* (*Chlamy* ChR1,

GenBank ID: 15811379), ChR2 from *Chlamydomonas reinhardtii* (*Chlamy* ChR2, GenBank ID: 158280944), ChR2 from *Volvox carteri* (*Volvox* ChR2, UniProtKB ID: B4Y105), ChR1 from *Volvox carteri* (*Volvox* ChR1, UniProtKB ID: B4Y103), ChR1 from *Mesostigma viride* (*Mesostigma* ChR, GenBank ID: 338176939), sensory rhodopsin II from *Natronomonas pharaonis* (Sensory rhodopsin II, PDB ID: 3QAP), bacteriorhodopsin from *Halobacterium salinarium* (Bacteriorhodopsin, PDB ID: 1IW6), halorhodopsin from *Halobacterium salinarium* (Halorhodopsin, PDB ID: 1E12), and xanthorhodopsin from *Salinibacter ruber* (Xanthorhodopsin, PDB ID: 3DDL). The sequence alignment between C1C2, sensory rhodopsin II, bacteriorhodopsin, halorhodopsin, and xanthorhodopsin was created based on secondary structure matching (SSM) superposition, using the PDBeFold server[7]. The C-termini of *Chlamy* ChR1, *Chlamy* ChR2, *Volvox* ChR1, *Volvox* ChR2, and *Mesostigma* ChR are truncated. Secondary structure elements for C1C2 are shown as coils (α: α-helices, η: 3_{10}-helices) and arrows (β-strands). "TT" represents turns. Identical and conservatively substituted residues are highlighted in red (in blue box). Cysteine residues involved in dimerization are colored magenta. The three residues that form the internal gate are colored green. Tyrosine, which is buried in the putative pore exit, is colored yellow. Glutamate, the possible proton donor, is colored blue. Red and green asterisks under the alignment indicate the residues that form the conserved hydrophobic retinal-binding pocket and the conserved cluster at the extracellular vestibule of the cation-conducting pathway, respectively. Blue asterisks indicate the possible proton acceptors from the Schiff base.

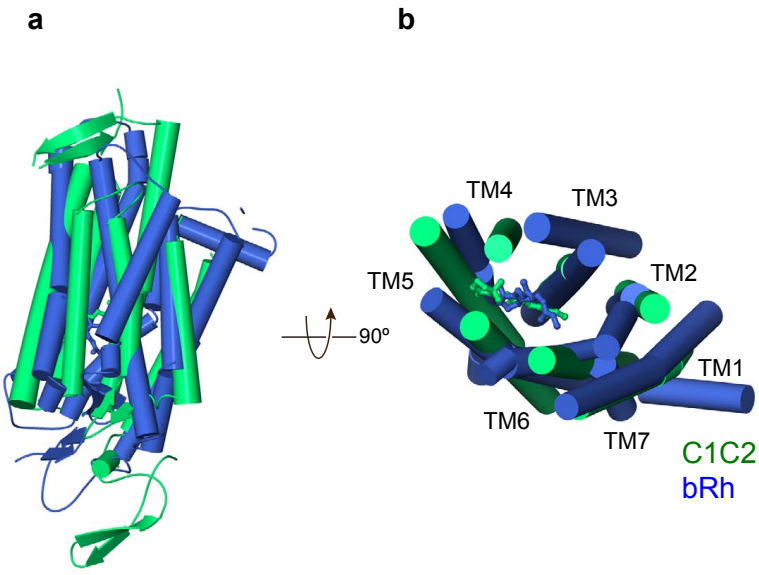

Supplementary Figure 5 | Structural comparison of C1C2 and bRh. a, b, Side view (**a**) and extracellular view (**b**) of the superimposed structures of C1C2 (green) and bRh (blue). Only seven-transmembrane regions are shown for clarity in (**b**).

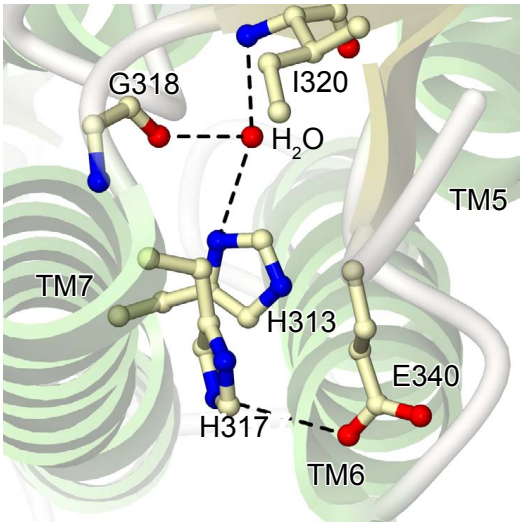

Supplementary Figure 6 | Interactions between the protruding part of TM7 and the C-domain. a, b, Interface between the protruding part of TM7 and the C-domain. Hydrogen bonds are shown by dashed lines.

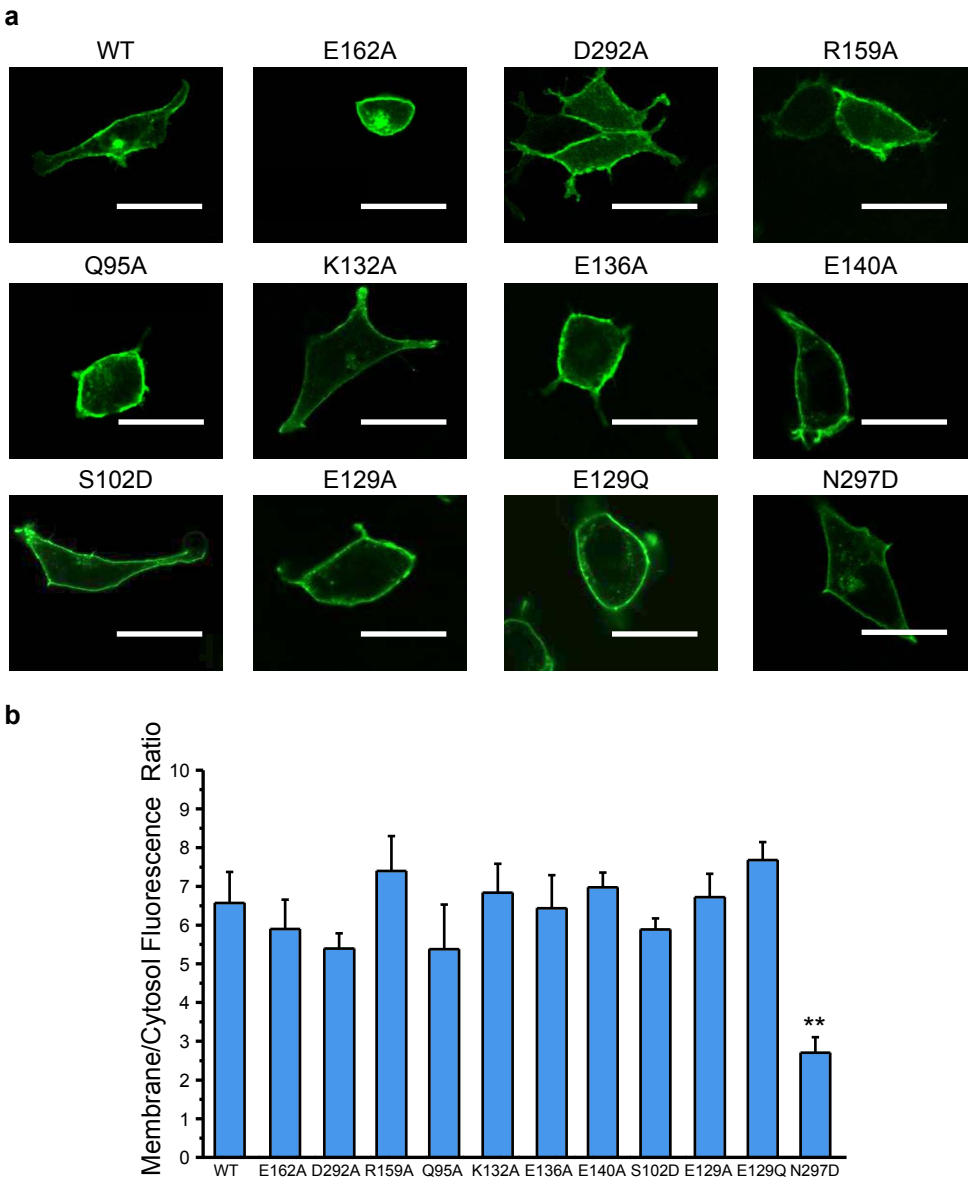

Supplementary Figure 7 | Membrane expression and localization of wild-type C1C2 and its mutants. a, Confocal images of representative HEK293 cells expressing the wild-type C1C2 and the its eleven mutants. Scale bar represents 30 μm. **b,** The expression level of wild-type C1C2 and the mutants quantified by membrane/cytosol fluorescence ratio. Values are means and SEM of 12-49 cells. **: $p<0.01$.

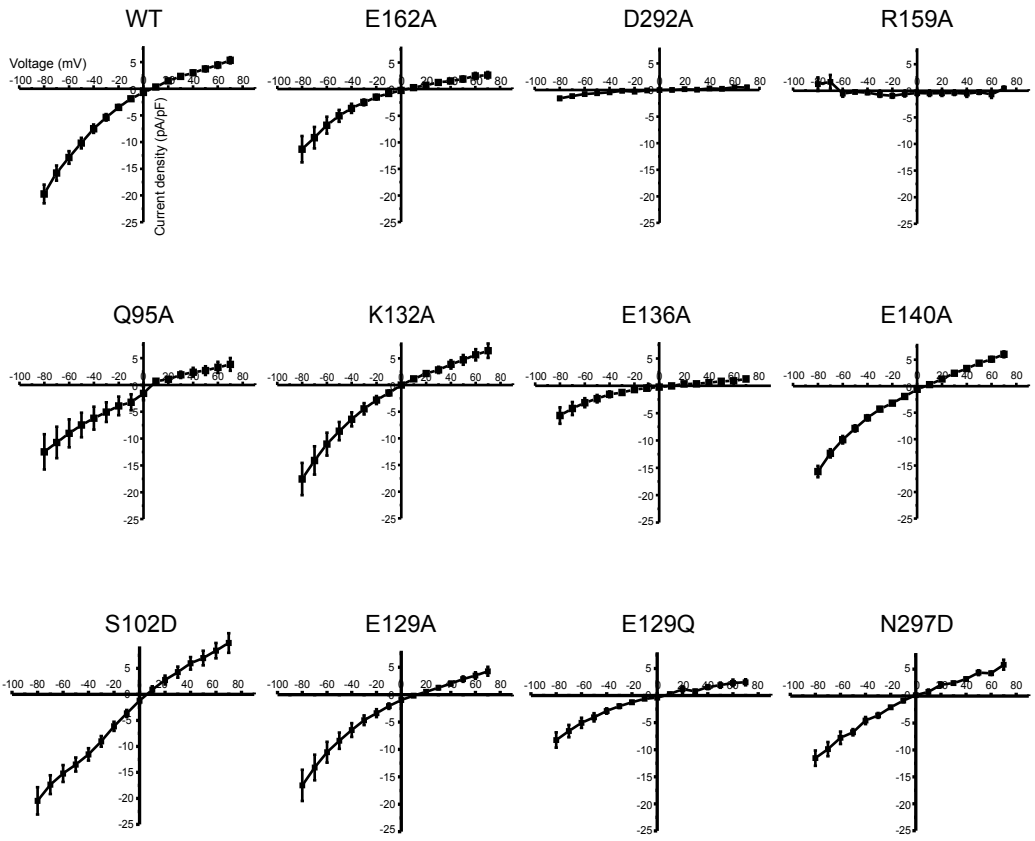

Supplementary Figure 8 | The current-voltage relationships of wild-type C1C2 and its mutants. The current-voltage (I-V) relationship between -70 and + 80 mV was determined from the single current amplitude at the indicated potentials. Values are means and SEM of 4-15 experiments. Extracellular solution: 145 mM NaCl, 1 mM $CaCl_2$, 2 mM $MgCl_2$, 10 mM HEPES, 5 mM glucose, pH 7.4. Intracellular solution: 140 mM KCl, 5 mM EGTA, 2 mM $MgCl_2$,10 mM HEPES, pH 7.4.

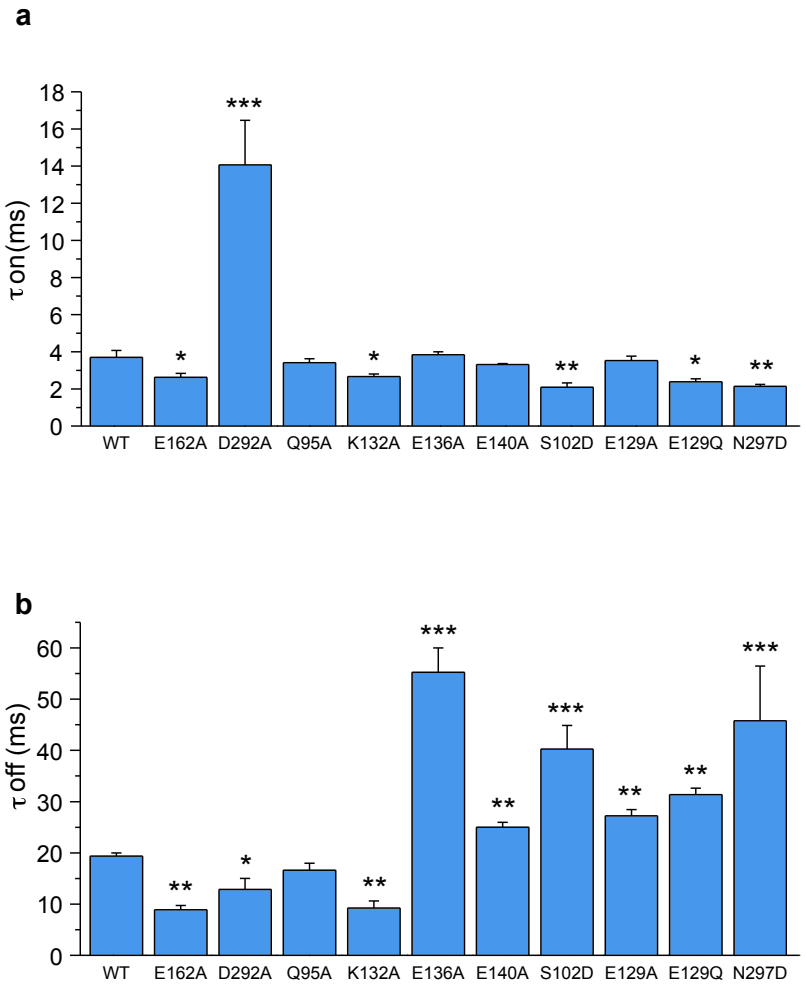

Supplementary Figure 9 | Photocurrent kinetics of wild-type C1C2 and its mutants. a, Opening rates (τ_{ON}) and **b,** closing rate (τ_{OFF}) of wild-type C1C2 and 10 mutants. Because of the weak photocurrent, the kinetics of the R159A mutant could not be measured. Values are means and SEM of 4-15 experiments. *: p<0.05, **: p<0.01, ***: p<0.001.

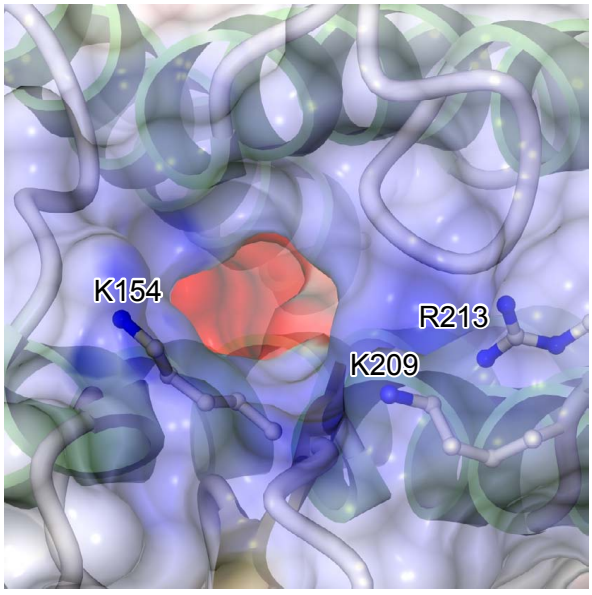

Supplementary Figure 10 | Slightly electropositive surface around the extracellular vestibule. The extracellular vestibule is shown formed by the N-domain and ECL1-3.

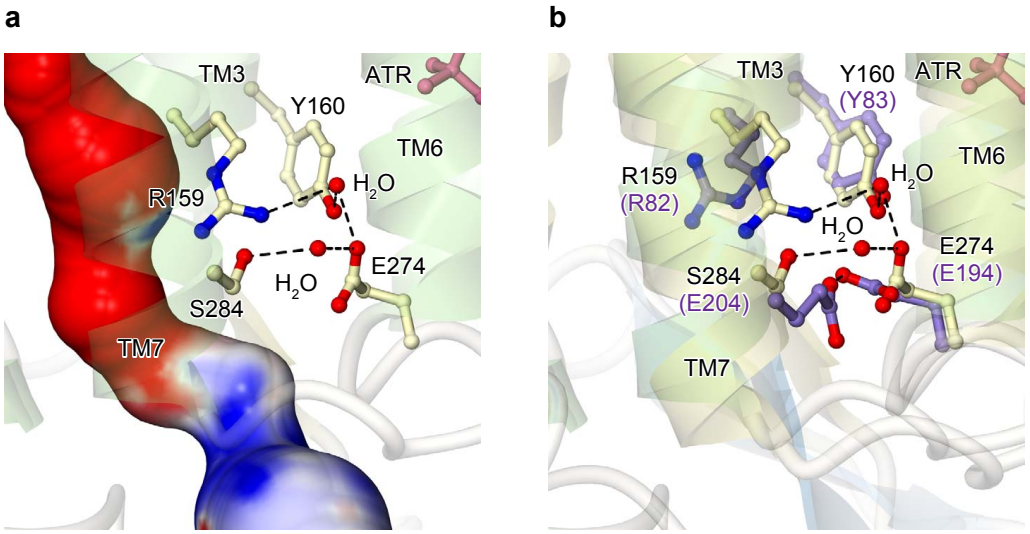

Supplementary Figure 11 | Conserved cluster near the extracellular vestibule. a, Conserved cluster formed by Arg159 (120), Tyr160 (121), Glu274 (235), and Ser284 (245) and water molecules. **b,** Structural comparison of the extracellular vestibules between C1C2 and BR. BR residues are colored in purple, and corresponding numbering is shown in parenthesis.

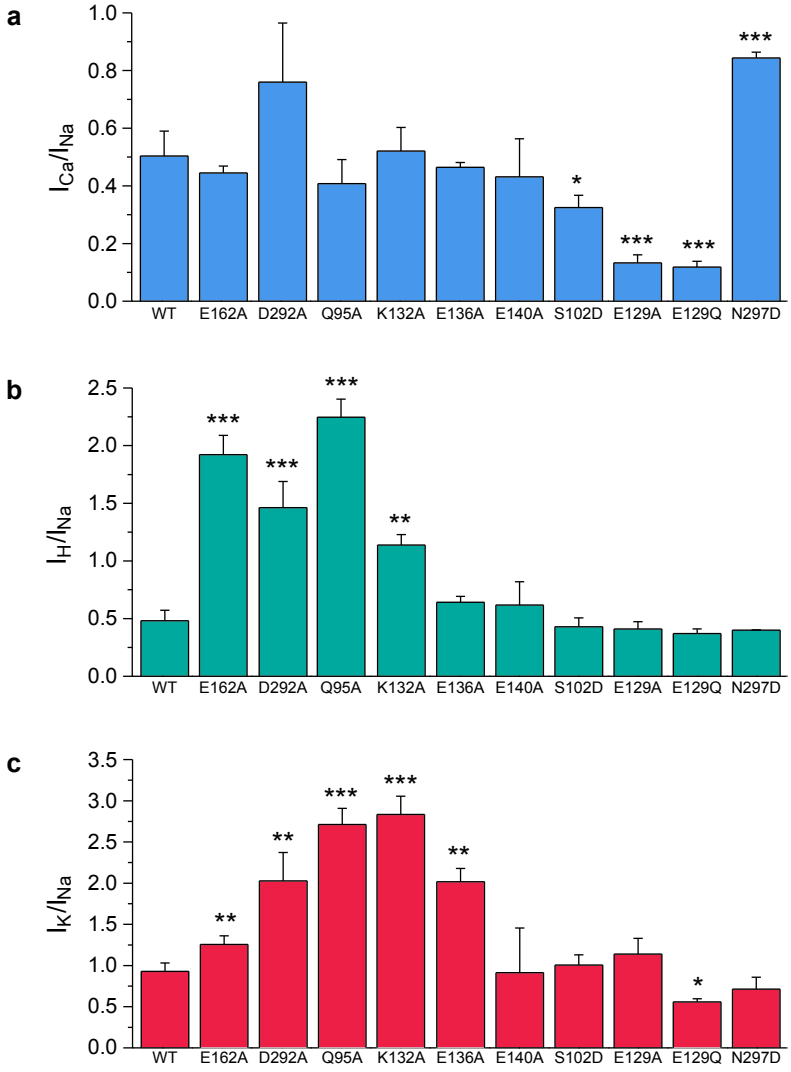

Supplementary Figure 12 | The ions selectivity of wild-type C1C2 and its mutants. The ratio of photocurrents carried by **a,** Ca^{2+} and Na^+; **b,** H^+ and Na^+; and **c,** K^+ and Na^+. Because of the weak photocurrent, ion selectivity of the R159A mutant could not be measured. Values are means and SEM of 4-15 experiments. *: $p<0.05$, **: $p<0.01$, ***: $p<0.001$. Similar ion composition as in Supplementary Figure 8 except NaCl was replaced by KCl (140 mM) or $CaCl_2$ (90 mM) or NMDG (135 mM + 5 mM NaCl), pH 6.4.

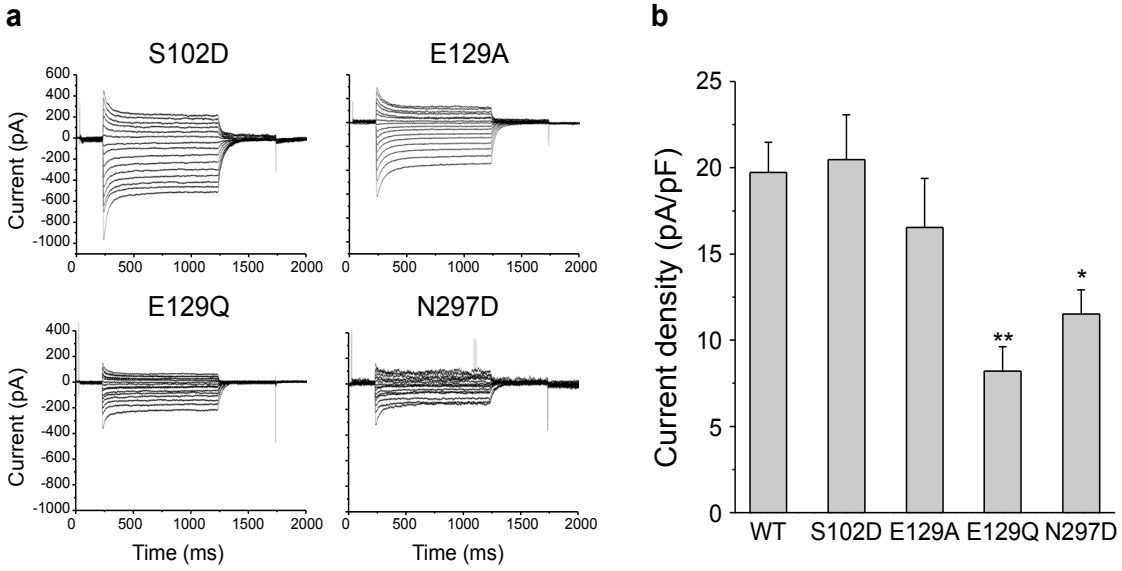

Supplementary Figure 13 | The photocurrents of wild-type C1C2 and its gating mutants. a, Effects of the mutations of S102, E129, and N297 on photocurrent. **b,** The peak amplitudes of the photocurrents, normalized by cell capacitance. Values are means and SEM of 4-8 experiments. *: $p<0.05$, **: $p<0.01$.

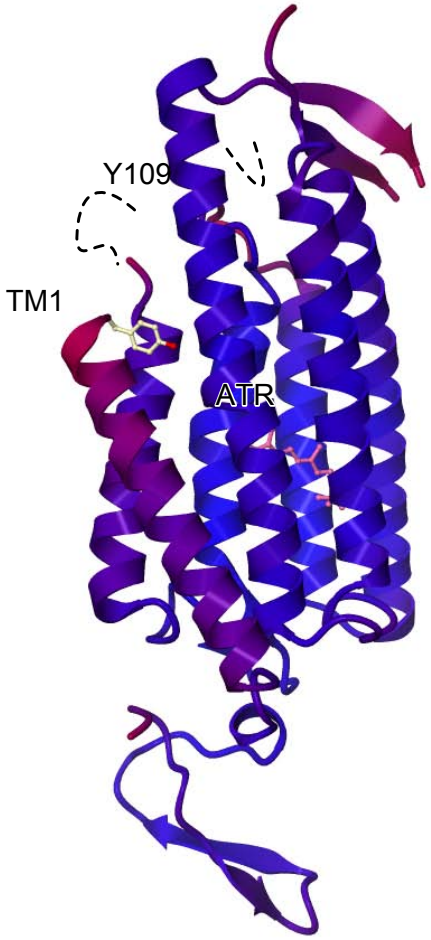

Supplementary Figure 14 | B-factor distribution of C1C2. B-factor distribution of the C1C2 monomer. The B-factors are colored in a gradient varying from blue (the lowest values) to red (the highest values). Disordered regions are shown as dotted lines.

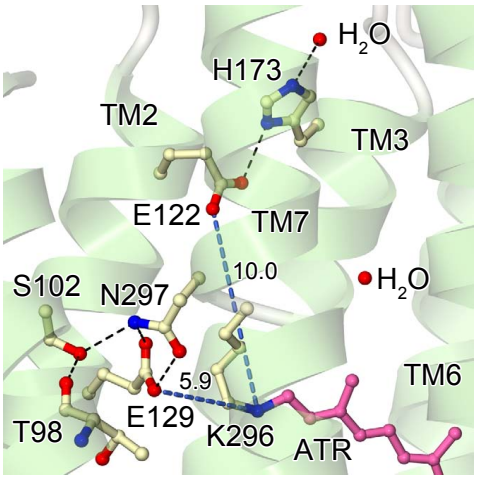

Supplementary Figure 15 | Putative proton donors to the retinal Schiff base. The distances between the Schiff base and the putative proton donors, Glu122 and Glu129, are shown as dotted blue lines. Hydrogen bonds are shown by dotted black lines.

Supplementary Table 1. Data collection, phasing and refinement statistics of C1C2

	Native (X06SA)	MeHgCl (BL32XU)		
Data collection				
Space group	$C222_1$	$C222_1$		
Cell dimensions				
a, *b*, *c* (Å)	59.5, 139.1, 90.0	59.7, 142.0, 93.4		
		Peak	*Inflection*	*Remote*
Wavelength	0.979500	1.00000	1.00939	1.01300
Resolution (Å)	50.0-2.30	39.0–3.20	39.0–3.28	39.1-3.41
	(2.44-2.30)	(3.38–3.20)	(3.46–3.28)	(3.59-3.41)
R_{sym}	8.0 (93.6)	30.4 (92.7)	28.2 (108.3)	24.2 (88.4)
$I/\sigma(I)$	16.5 (1.9)	17.8 (3.7)	13.4 (2.9)	11.2 (3.4)
Completeness (%)	97.9 (95.6)	99.0 (97.5)	99.1 (98.8)	99.0 (97.6)
Redundancy	6.6 (6.5)	35.3 (18.2)	22.5 (13.1)	12.0 (12.2)

*Highest resolution shell is shown in parentheses.

Supplementary Table 1. Data collection, phasing and refinement statistics of C1C2 (continued)

	Crystal
Refinement	
Resolution (Å)	36.6-2.30
No. reflections	16709
R_{work}/R_{free}	0.2040/0.2512 (0.2157/0.2532)
No. atoms	
Protein	2187
Lipid	65
Ligand (ATR)	20
Average *B*-factors (Å^2)	
Protein	51.3 (47.9)
Lipid	68.0 (56.4)
Ligand (ATR)	43.6 (39.9)
Coordinates error (Å)	0.78 (0.72)
R.m.s. deviations	
Bond lengths (Å)	0.008 (0.008)
Bond angles (°)	1.306 (1.327)

*Statistics without the TLS refinement are shown in parentheses.

Supplementary Table 2. pKas calculated using PROPKA

Residue name	Calculated-pKa	Model-pKa
Asp292	3.21	3.80
Glu122	8.33	4.50
Glu129	9.31	4.50
Glu162	5.83	4.50
His173	1.33	6.50